Instruments and Experimental Techniques, 2025, No

PHYSICAL INSTRUMENTS FOR ECOLOGY, MEDICINE, AND BIOLOGY

AEROSOL CHAMBER FOR MODELING ATMOSPHERIC PROCESSES

©2025. Hong-Da Tai[a], Wei Zhong[a,b], Yuan Wang[c,*], Yi Li[d], Zi-Bo Zhuang[a], Pak-Wai Chan[e]

[a]*Civil Aviation University of China, Tianjin, 300300 China*

[b]*Air Traffic Management Bureau of North China, Beijing, 102604 China*

[c]*Shandong Vocational University of Foreign Affairs, Shandong, 264504 China*

[d]*Shaanxi Institute of Metrology Science, Shanxi, 710100 China*

[e]*Hong Kong Observatory, Hong Kong, 999077 China*

e-mail: YuanWang55@outlook.com

Received ~~September 10~~ October 9, 2025; ~~4~~ revised May 5, 2025; accepted August 25, 2025.

Abstract – Simulated atmospheric process experiments in aerosol chambers can achieve shorter testing times and lower visibility levels than those typical for experiments in natural environments. In this paper, the design of an aerosol chamber is described, and the results of studies on its characteristics are presented. During the initial phase of the experiment, the rate of change in the extinction coefficient was relatively low, indicating a stable environment within the simulation chamber. Comparison of the stages with the slowest and fastest changes in extinction coefficient showed that during the slowest rate of change, the particle number concentration in the 0.28–0.40 μm size range exhibited greater variation, while during the fastest rate of change, the particle number concentration in the 0.40–2.00 μm size range showed more significant variation.

1. INTRODUCTION

Aerosol chambers that replicate extreme environments in a stable manner, such as constant-temperature tanks for platinum resistance temperature sensors and hygrostats for polymer film humidity sensors, are crucial for testing and calibrating meteorological sensors. In addition, some laboratories are capable of simulating various atmospheric processes. For example, the McKinley climatic laboratory, the world's largest support facility for environmental simulation testing, can simulate diverse conditions, such as extreme temperatures, high winds, snow, salt fog, sand, dust, humidity, freezing rain, icing, and solar radiation [1, 2]. However, the changes in visibility during

atmospheric process variations, especially the impact of aerosol changes on visibility, are still not fully understood. Visibility is the greatest distance at which a black object of suitable dimensions can be recognized against the horizon under standard lighting conditions. In aviation operations, the meteorological optical range (MOR) is often used as a proxy for visibility [3]. Therefore, our research focuses on the variations in low-visibility atmospheric processes due to large amounts of aerosols.

Maintaining the stability of an aerosol chamber is crucial when simulating atmospheric processes. An aerosol chamber is designed to simulate extreme weather events, and thus, extreme conditions must be maintained. The goal is to prolong the duration of these extreme processes as much as possible to provide sufficient time for experimental research. Therefore, an aerosol chamber must be able not only to generate extremely low-visibility environments but also to sustain them for extended periods.

In this paper, the development of an aerosol chamber designed for simulating atmospheric processes, particularly low-visibility atmospheric events, is presented. This chamber can be used for the rapid simulation of various aerosol types and low-visibility atmospheric conditions such as fog, haze, and dust storms. In the aerosol chamber, we simulated low-visibility atmospheric processes, measured the extinction characteristics and atmospheric transmittance using high-precision measurement devices [4], and evaluated the aerosol particle size distribution and its changes using an optical particle counter. The variations in the extinction coefficient and aerosol particle size distribution in the simulated low-visibility environment were analyzed and the stability of the aerosol chamber was further investigated. The findings can provide a scientific basis for constructing atmospheric environments under different weather conditions and exploring the variation in visibility with changes in atmospheric composition.

2. DESIGN

The aerosol chamber consists of several components, including an atmospheric environment simulation chamber, an equipment room, an air supply and circulation system, a monitoring room, a power supply system, and a water supply and drainage system. An external photo of the aerosol chamber is shown in Fig. 1a. The main structure of the aerosol chamber, the atmospheric environment

Fig. 1

simulation chamber, is a framework-type cylindrical structure built with laminated tempered glass (6 mm + 6 mm thickness), with the total glass area of 239.6 m². The internal cross-section of the chamber is rectangular, with the height of 1.69 m, width of 6 m, and overall length of 55.7 m. The floor of the chamber is made of reinforced concrete, which is poured onsite, with high-quality corrosion-resistant outdoor tiles. The surfaces of the tiles are coated with green epoxy floor paint. Drainage channels and outlets are located at the bottom of the passage walls. All internal pipelines in the chamber are made of PVR pipes. A physical image of the interior of the simulation chamber is shown in Fig. 1b.

The central part of the aerosol chamber houses an equipment room—an open, single-story space standing 2.476 m tall—dedicated to housing a suite of advanced aerosol generation and detection instruments, as shown in Fig. 2. Among the installed devices is the SAG-410/L dust generator from TOPAS (Germany), which produces high-concentration size-controlled solid aerosol particles; its modular design supports various powders, allows for low-flow, high-concentration output, and enables powder replacement during operation—making it ideal for long-duration testing. The Jingcast 5201A black carbon aerosol generator (Jingcast, Switzerland) specializes in producing stable black carbon particles derived from vehicle exhaust or biomass combustion. The ATM-241 aerosol atomizer (TOPAS, Germany) efficiently converts liquid samples into uniform aerosol droplets, serving as a key component for generating stable aerosols. The DUSTTRAK II 8530 dust monitor (TSI, USA) provides real-time monitoring across multiple particle size fractions (PM1/2.5/10) and features auto-zeroing, data logging, and alarm capabilities. The Grimm 1.109 particle size spectrometer (Grimm, Germany) uses light-scattering techniques to deliver high-resolution real-time particle size distribution profiles critical for detailed analysis. Finally, the EAN-581 aerosol electrostatic neutralizer (TOPAS, Germany) neutralizes particle charge state, ensuring accuracy and consistency throughout sample transportation and measurement. Together, this integrated setup underpins high-precision reliable aerosol simulation, monitoring, and control–forming an essential experimental foundation for low-visibility weather simulation and related environmental research.

The side of the aerosol chamber is equipped with 10 aerosol inlets and 6 exhaust outlets, all located on the same side of the chamber. The inlets are spaced 5 m apart with the center of each inlet

0.9 m above the chamber floor. The diameter of each inlet is 25 mm. The 6 exhaust outlets are divided into two groups with 3 outlets in each group. The first outlet of the first group is located 6 m from the starting end of the chamber, whereas the first outlet of the second group is located 38 m from the starting end. The bottom of the exhaust outlets is 10 cm above the floor and the outlet diameter is 12 cm. Aerosol particles are generated by the ATM-241 aerosol generator and transported through pipes to the aerosol inlets, where the particles are injected into the chamber. In the pipe design, the number of bends included is minimized and a larger pipe diameter is used to reduce the likelihood of water vapor and aerosol particles adhering to the pipe walls. The aerosol inlets are located at the pipe bends and each inlet is equipped with an anemometer to measure the wind speed. Through the adjustment of the valves, the wind speed at each inlet is kept constant, ensuring the uniform release of aerosol particles throughout the chamber.

The aerosol supply and circulation system run throughout the entire atmospheric simulation chamber. Aerosols are injected into the chamber by an air compression system, which transports the gases generated by the aerosol generation equipment to the central part of the chamber. To prevent the aerosol particles from settling, 10 sets of AC fans and ventilation ducts are installed on the opposite side of the aerosol inlets and exhaust outlets at the bottom of the chamber. In Fig. 1b, the blue circular component and white square located in the lower-left region represent recirculation ducts designed to facilitate airflow circulation. Each fan has the diameter of 20 cm and the ventilation duct size is 23 cm × 23 cm. The fans are directly connected to the ducts within the chamber walls, creating the localized circulation of airflow at the bottom of the chamber. The first set of fans is located 7.25 m from the starting end of the chamber with the center of the fan being 1 m away from the center of the ventilation duct. The two sets of fans are spaced 5 m apart and the fan centers are 19 cm above the floor. The rotational speed of the fans is 2500 rpm and the flow rate of the fans is 12 m^3/min. The time required for the airflow inside the chamber to achieve uniform mixing is less than 30 min (measured by dust monitors at the front, middle, and rear of the chamber, with the reading difference of less than 5 μg/m^3). The aerosol chamber is equipped with a complete air circulation system, ultrasonic atomization generators, and smoke and black carbon aerosol generators. This setup can reduce visibility from 10,000 m to less than 3,000 m within 1.2 h and further decrease it to less than 200 m

within 5 h. This allows the aerosol chamber to simulate various low-visibility weather conditions, such as fog and haze, while shortening the testing period.

A large exhaust fan is installed on one sidewall of the aerosol chamber to remove aerosols and smoke from the chamber. In Fig. 3, the outlined white section is the air intake of the axial-flow fan used for purifying the laboratory air. In addition, a filtration system is added to the air intake of the aerosol chamber to ensure that the air entering the chamber is clean. This system allows the low-visibility environment to be quickly restored to a normal, clean state. The performance parameters and their corresponding values of the simulation chamber are presented in Table 1.

3. MODELING PROCESS AND RESULTS

Although there has been extensive research on fog, studies on haze are relatively limited. Indoor simulation of haze helps in evaluating the performance of visibility instruments in a haze environment [5, 6]. Therefore, an indoor haze simulation experiment was conducted in the aerosol laboratory. In the experiment, measurements were taken for approximately 4 h, from 21:13 to 1:22. In this experiment, we simulated an aerosol environment characterized by small particles in the size range of 0.28–2.50 μm under low relative humidity conditions (RH < 80%), which closely aligns with the characteristics of extreme haze events in nature [7, 8]. Considering the high proportion of NH_4^+ and SO_4^{2-} in the atmospheric composition of China, in this study, $(NH4)_2SO_4$ was primarily used as the aerosol component [9]. Aerosol particles were continuously injected into the system at a constant rate using a TOPAS ATM241 system, producing polydisperse particles primarily smaller than 1 μm, with the median size of 0.5–1 μm, using $(NH4)_2SO_4$ in deionized water. To ensure the accuracy of the experiment, the aerosol particle size spectrometer was consistently placed in a relatively uniform area in the simulated haze environment, as the uniformity of the simulation chamber environment had been previously validated [4]. Throughout the experiment, the temperature inside the chamber was kept constant. During the experiment, an ATM-241 generator was continuously used to inject aerosol particles into the simulation chamber, simulating the process of decreasing atmospheric visibility. Simultaneously, a Grimm 1.109 particle size spectrometer was used to record the size distribution of the aerosol particles.

As aerosol particles are injected into the simulation chamber, the indoor visibility gradually decreases and the extinction coefficient gradually increases. Fig. 4a, b shows the variation in aerosol particle number concentration with decreasing visibility for different particle size ranges, with different colors corresponding to different size ranges. Fig. 5 shows the variation in the extinction coefficient during the experiment. As shown in Figs. 4 and 5, the particle number concentration in the 0.28–0.65 μm size range is much greater than that in the 0.65–2.5 μm size range. In the 0.35–2.5 μm size range, the particle number concentration first increases but then decreases, whereas in the 0.35–2.5 μm size range, the particle number concentration tends to increase with time, and the extinction coefficient continues to increase over time. However, Fig. 4 shows raw data from the experiment (rather than normalized data), resulting in distorted images.

Fig. 4–6

Fig. 6a–e shows the correlations between extinction coefficients and number concentrations in different size ranges. The scatter plots in the figure represent the particle number concentrations at different visibility levels, whereas the straight line illustrates the correlation between the extinction coefficient and the particle number concentration.

The particle number concentration is found to be the main factor affecting the extinction coefficient. Fig. 6a–e shows that the number concentration is most strongly correlated with the extinction coefficient when the particle size is greater than 0.58–1 μm and that the correlation coefficients consistently exceed 0.9 with the particle number concentration in the particle size range of 0.7–0.8 μm showing an exceptionally high correlation (0.994) with the extinction coefficient. For the ranges of 0.40–0.58 μm and 1–2.0 μm, the correlation coefficients are greater than 0.8. The particle number concentration within the particle size range of 0.58–2 μm increases with increasing extinction coefficient. However, when the particle size is greater than 2.0 μm or is in the range of 0.28–0.35 μm, the number concentration is weakly correlated with the extinction coefficient with correlation coefficients all less than 0.5. Specifically, the particle number concentration within the range of 0.28–0.3 μm shows a correlation of only 0.211 with the extinction coefficient. For particle sizes ranging from 0.4 to 2 μm, the number concentration has a close relationship with the extinction coefficient with correlation coefficients above 0.8.

We used an aerosol PAS1.109 spectrometer to measure aerosol particle size distributions, which,

in the atmospheric simulation chamber, were essentially consistent with the Deirmendjian modified gamma distributions. We employed normalized histograms to characterize the variations in aerosol number concentration across different size ranges. These histograms were generated on the basis of data collected from 21:13 to 0:38, capturing the temporal trends of aerosol particles of varying diameters. The resulting frequency functions are depicted in Fig. 7a, b, where the x-axis represents the diameter of the aerosol particles and the y-axis is expressed as a fraction, calculated as the width of each rectangle divided by the total number of particles; this provides a comprehensive overview of the aerosol particle size distribution within the simulation chamber under varying visibility conditions. As shown in Fig. 7, the generated aerosol particle size is mainly concentrated in the range of 0.01–1 μm. For particles with sizes greater than 1 μm, it is difficult for the particle size to increase because of the slow growth rate and the proportion of the number concentration is very small and basically unchanged.

Fig. 7, 8

4. STABILITY OF THE AEROSOL CHAMBER

With the normalization of the data, the impact of aerosol particle size on the extinction coefficient can be assessed for different size ranges, as shown in Fig. 8. In the figure, different colors represent the percentages of different size particles in the aerosol composition for the certain extinction coefficient. The size of the bubbles indicates the particle content in the total composition within that size range with larger bubbles indicating higher content and vice versa. For example, the percentages of particles in different size ranges in the total particle composition for the extinction coefficient of 0.0005 are shown in Table 2.

The particle size distribution shown in Fig. 8 follows the Modified Gamma Distribution [10, 11]. The analysis of the results from the figure indicates that the modal radius falls within the range of 0.28 to 0.35 μm [12]. Initially, with increasing extinction coefficient and decreasing visibility, the total composition of the 0.28 to 0.35 μm diameter particles is the highest, especially that of the 0.28 to 0.30 μm diameter particles, which account for 21.4% to 50.3% of the total composition. However, as the extinction coefficient further increases, the number of particles in the 0.28 to 0.35 μm range gradually decreased, whereas that in the 0.35 to 2.00 μm range increases.

The variation in the extinction coefficient is closely related to the temporal evolution of the aerosol particle size distribution and the change in the particle size distribution strongly affects the extinction coefficient. The main factor contributing to the increase in the extinction coefficient is the shift in the main particle size range from 0.28 to 0.35 μm to 0.35 to 2.00 μm. Figs. 4 and 8 show that the particle number concentration in the 0.28 to 0.35 μm range is significantly greater than that in the 0.35 to 2.00 μm range. Particles in the 0.28 to 0.35 μm range have greater impact on the extinction coefficient. However, as time progresses, the particle number concentration in the 0.28 to 0.35 μm range begins to decrease, whereas the concentration in the 0.35 to 2.00 μm range, although small, tends to increase. Yan et al. [13] reported that larger aerosol particles have larger extinction coefficient than smaller aerosol particles do. Therefore, in the 0.35 to 2.00 μm range, the larger the particle radius is, the more significant its contribution to the extinction coefficient is. This observation is consistent with the findings of Yan et al. [13].

Fig. 9

The normalized data were processed to obtain the average rates of change per minute in the extinction coefficient and particle number concentration in the different periods, as shown in Fig. 9. The experimental results show that the rates of change in the aerosol particle number concentrations exhibit different characteristics across the different particle size ranges. The rate of change in the aerosol particle number concentration in the range of 0.28 to 0.65 μm is relatively large, possibly because of collision and aggregation effects among the aerosol particles. These smaller aerosol particles are more easily influenced by air flow and remain suspended in the air, leading to a more significant change in their number concentration. In contrast, in the range of 0.65 to 2.50 μm, as the particle size increases, the rate of change in the particle number concentration gradually decreases and remains nearly constant; this effect may be related to the settling rate of the aerosol particles, where larger particles settle faster and are more likely to deposit on the ground or surfaces. In particular, in the range of 1.30 to 2.50 μm, the rate of change in the particle number concentration approaches zero; thus, the settling rate of these particles is very fast. In this experiment, the proportion of particles with a size greater than 2.5 μm can be neglected and the rate of change in the number concentration is considered zero.

Between 21:13 and 22:42, the change in the extinction coefficient is slow, at a rate of $1.45 \cdot 10^{-5}$,

while the particle number concentration in the 0.28–0.58 μm size range changes significantly. During the period from 22:42 to 22:51, the rate of change in the extinction coefficient is $1.05 \cdot 10^{-4}$ and simultaneously, the rate of change in the number concentration in the 0.30–0.58 μm size range peaked. Further observations during the period from 23:45 to 23:54 reveal the fastest rate of change in the extinction coefficient, at $1.16 \cdot 10^{-4}$, with the significant rate of change in the particle number concentration in the 0.28–0.58 μm size range. Comparison of the periods with the slowest and fastest changes in the extinction coefficient reveals that the change in the particle number concentration in the 0.28–0.40 μm size range is 7 times greater in the former than in the latter. In contrast, in the 0.40–2.00 μm size range, the particle number concentration rate of change is greater in the latter period than in the former. In the particle size range of 0.40 to 1.30 μm, as the particle size increases, the rate of change in the number concentration gradually increases, reaching a peak within the range of 1.00 to 1.30 μm. At this point, the slowest rate of change in the extinction coefficient corresponds to the rate of change in concentration of 0.012 $m^{-3} \cdot min^{-1} \cdot \mu g$ whereas the fastest rate of change in the extinction coefficient corresponds to the rate of change in concentration of 19.23 $m^{-3} \cdot min^{-1} \cdot \mu g$; this result is likely related to the continuous injection of aerosol particles into the room during the experiment.

The main purpose of the atmospheric simulation chamber is to test and calibrate visibility instruments, and the extinction coefficient is considered the key physical parameter for evaluating visibility instruments such as atmospheric transmissometers. Therefore, the stability requirements of the simulated environment actually translate to the requirements regarding the stability of the extinction coefficient within the chamber. Stable extinction coefficient ensures the accuracy and reliability of the test results, thereby ensuring the precision of the instruments in measuring visibility. The experimental data indicate that during the initial stage of the experiment, from 21:13 to 22:42, the rate of change in the extinction coefficient is relatively small, indicating good extinction coefficient stability and a relatively stable environment within the simulation chamber. Comparison of the minimum and maximum values of the rate of change in the extinction coefficient reveals that the rate of change in the particle number concentration in the 0.28–0.40 μm size range is greater in the former than in the latter, whereas in the 0.40–2.00 μm range, the rate of change in the particle number concentration is greater in the latter than in the former. This finding indicates that the rapid change in

the extinction coefficient within the chamber is influenced mainly by the change in the particle number concentration in the 0.40–2.00 μm size range.

5. CONCLUSION

In this paper, the structure of an aerosol chamber designed to simulate atmospheric processes and the functions of its various components are introduced. An experiment was conducted within the aerosol chamber. Through the analysis of the variations in the extinction coefficient and particle number concentration, the characteristics of the aerosol chamber were studied. During the initial phase of the atmospheric simulation (21:13–22:42), the rate of change in the extinction coefficient was relatively small, at $1.45 \cdot 10^{-5}$ min^{-1}, indicating that the aerosol chamber environment was stable at the beginning of the experiment. In this study, an atmospheric simulation environment with spatial uniformity and measurement stability capable of generating varying visibility conditions within 4 h was established. This haze simulation only represents the results of this experiment. In the future, different aerosol generators for various particle size ranges can be installed in the laboratory to enrich and expand our work.

STATEMENTS AND DECLARATIONS

FUNDING

This work was supported by the National Natural Science Foundation of China [Grant No. 41905129], the Open Project of the Key Laboratory of Metrological Optics and Application for State Market Regulation [Grant No. SXJL2023006KF], the Science and Technology Project of the Shaanxi Market Supervision Administration [Grant No. 2021KY01], the General Project of the Shaanxi Key Research and Development Plan [Grant No. 2022GY-320], and the Science and Technology Program of the State Administration for Market Regulation [Grant No. 2022MK120].

CONFLICT OF INTEREST

The authors have no conflicts of interest to declare.

Author Contributions

HDT conceived and designed the experiments and contributed to the analysis of the results. WZ and YW wrote the paper and generated the figures. YL, ZBZ and PWC were involved in the

discussions and helped with the data analysis.

REFERENCES

1. Drake, C., in *23rd Aerospace Sciences Meeting*, Reno, N.V., Ed., Orlando, FL: American Institute of Aeronautics and Astronautics, 1985, p. 89.
2. Hendrickson, C. *Flight Testing under Extreme Climatic Conditions.* Report for the US Air Force, Report No. AFFTC-TIH-88-004, California, CA: AFFTC-TIH, 1988.
3. World Meteorological Organization. 2021. Guide to Instruments and Methods of Observation (WMO-No. 8). Geneva: World Meteorological Organization.
4. Tai, H.D. *Research on Key Technologies for Visibility Instrument Testing and Evaluation*, Hefei, China: University of Science and Technology of China, 2020.
5. Wei, C., Zeqiang, B., Chu, J., Xiaolei, H., Dandan, J. *A method for calibrating forward scatter meters indoors.* [J]. Metrologia, 2020, 57(6): 065030. http://doi.org/10.1088/1681-7575/ab993e
6. Chan, P.W. *A test of visibility sensors at Hong Kong international airport.* [J]. Weather, 2016, 71(10): 241-246.
7. Liu, A., Wang, H., Cui, Y., Shen, L., Yin, Y., Wu, Z., Guo, S., Shi, S., Chen, K., Zhu, B., et al. Atmosphere, 2020, vol. 11, p. 56. https://doi.org/10.3390/atmos11010056.
8. China Meteorological Administration, Observation and Forecasting Levels of Haze, (QX/T 113-2010), China Meteorological Press, Beijing, 2010.
9. Deng, X.L., Shi, C.E., Wu, B.W., Yang, Y.J., Jin, Q., Wang, H.L., Zhu, S., and Yu, C. J. Environ. Sci., 2016, vol. 42, p. 32. https://doi.org/10.1016/j.jes.2015.07.010.
10. Petty, G.W., Huang, W. *The modified gamma size distribution applied to inhomogeneous and nonspherical particles: Key relationships and conversions*. [J]. J. Atmos. Sci., 2011, 68(7): 1460-1473. http://dx.doi.org/10.1175/2011JAS3645.1
11. Tampieri, F., Tomasi, C. *Size distribution models of fog and cloud droplets in terms of the modified gamma function.* [J]. Tellus, 1976, 28(4): 333-347.

12. Sun, Y., Zhou, X., Wang, W. *Aerosol size distributions during haze episodes in winter in Jinan, China.* [J]. Particuology, 2016, 28: 77-85. https://doi.org/10.1016/j.partic.2015.12.001
13. Yan, F., Hu, H., and Yu, T., *China Particuology*, 2004, vol. 2, p. 25. https://doi.org/10.1016/S1672-2515(07)60016-5

TABLES

Table 1. Performance parameters and values of the simulation chamber

Parameter	Value
Visible spectrum transmittance of chamber walls	>90%
Infrared spectrum transmittance of chamber walls	>70%
Maximum air volume, m^3/h	90
Fan wind speed, rpm	2500
Fan air volume, m^3/min	12
Operating parameter of compressed gas volumetric spray, m^3/min	0.1
Aerosol generator model	*ATM* 241
Uniform aerosol phase distribution range	x = 0.4 m ~ 1.2 m $y = 2.5 + n \cdot 5$ (n = 0, 1, 2 … 10) m z = 0.7 m ~ 1.1 m
Duration of the environmental stability, min	30

Table 2. Percentage of particles in different size ranges at the extinction coefficient of 0.0005

Particle Size Range, μm	Percentage, %
0.28–0.30	50.300
0.30–0.35	20.700
0.35–0.40	16.400
0.40–0.45	7.400
0.45–0.50	3.300
0.50–0.58	1.400
0.58–0.65	0.400
0.65–0.70	0.130
0.70–0.80	0.050
0.80–1.00	0.010
1.00–1.30	0.005
1.30–1.60	0.003
1.60–2.00	0.002
2.00 –2.50	0.001
2.50–3.00	0.008

FIGURE CAPTIONS

Fig. 1. Photographs of the exterior and interior layout of the aerosol chamber.

Fig. 2. Equipment room and aerosol generation instrumentation.

Fig. 3. Actual photo of the exhaust fan.

Fig. 4. **a)** Time series of the extinction coefficient and aerosol concentration of the 0.28–0.3 μm, 0.3–0.35 μm, 0.35–0.4 μm, 0.4–0.45 μm, 0.45–0.5 μm, 0.5–0.58 μm, and 0.58–0.65 μm particles. **b)** Time series of the extinction coefficient and aerosol concentration of the 0.65–0.7 μm, 0.7–0.8 μm, 0.8–1 μm, 1–1.3 μm, 1.3–1.6 μm, 1.6–2 μm, and 2–2.5 μm particles.

Fig. 5. Variation of the extinction coefficient with respect to time.

Fig. 6. Correlations between the extinction coefficients and numerical concentrations of the aerosols in the different size ranges.

Fig. 7. **a)** Fraction/μm versus particle sizes of 0.28–0.3 μm, 0.3–0.35 μm, 0.35–0.4 μm, 0.4–0.45 μm, 0.45–0.5 μm, 0.5–0.58 μm, and 0.58–0.65 μm. **b)** Fraction/μm versus particle sizes of 0.65–0.7 μm, 0.7–0.8 μm, 0.8–1 μm, 1–1.3 μm, 1.3–1.6 μm, 1.6–2 μm, and 2–2.5 μm.

Fig. 8. Relationship between the aerosol particle size and extinction coefficient.

Fig. 9. Relationship between the change rate of the extinction coefficient and the change rate of the particle number concentration.

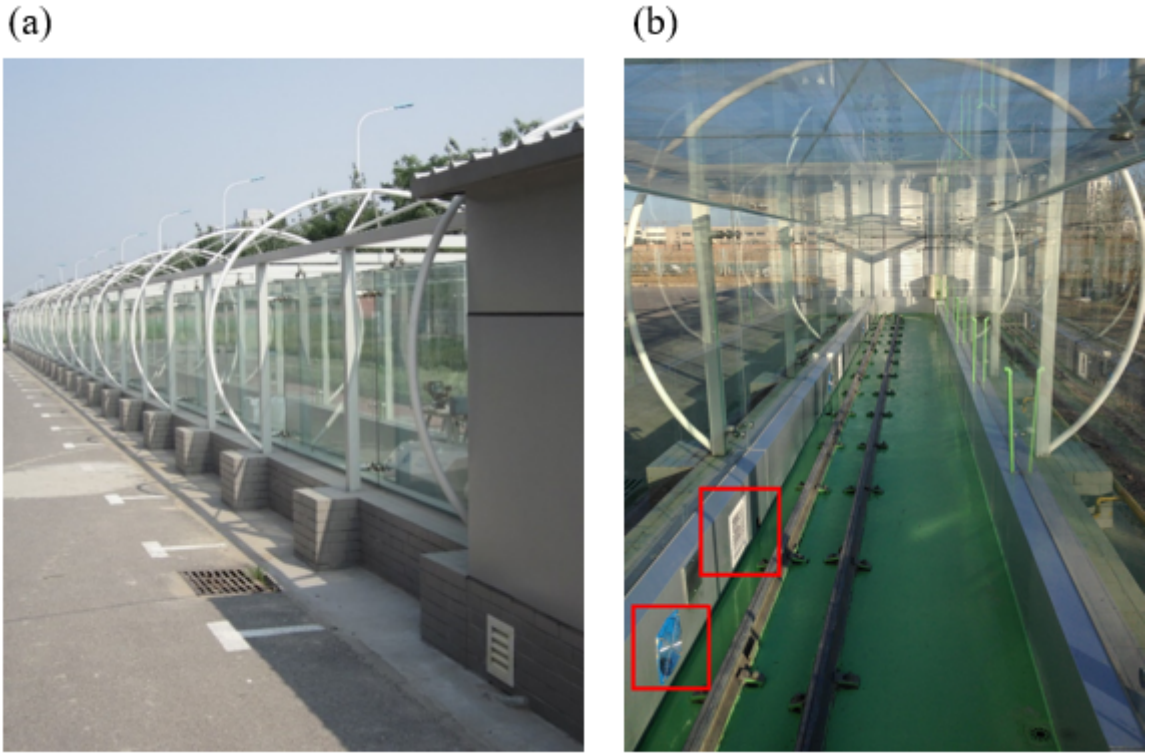

Fig. 1.

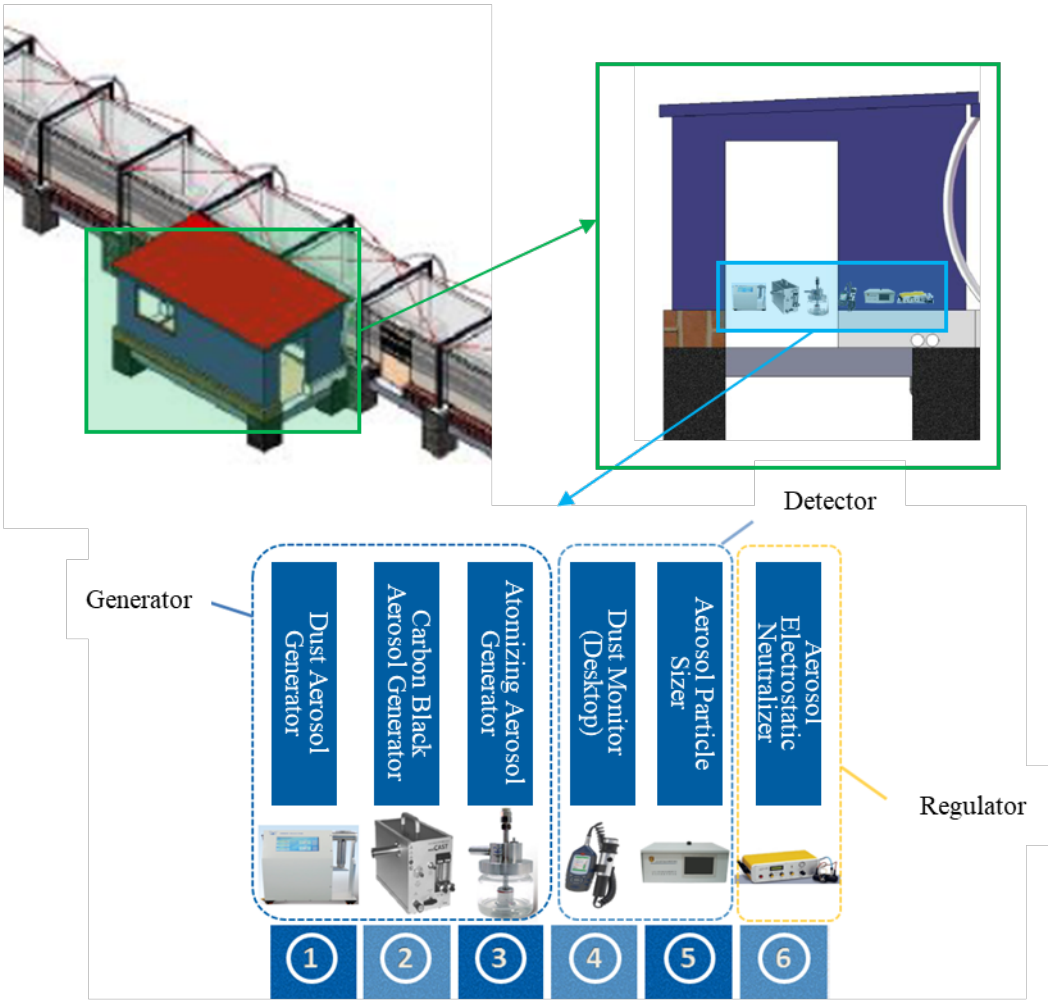
Detector
Generator
Dust Aerosol Generator
Carbon Black Aerosol Generator
Atomizing Aerosol Generator
Dust Monitor (Desktop)
Aerosol Particle Sizer
Aerosol Electrostatic Neutralizer
Regulator
1
2
3
4
5
6

Fig. 2.

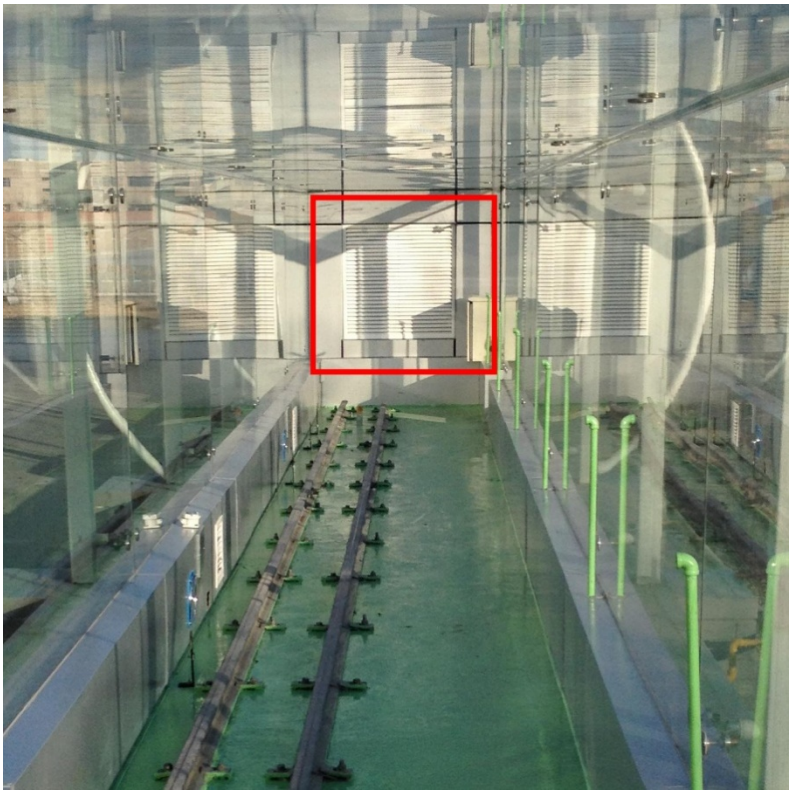

Fig. 3

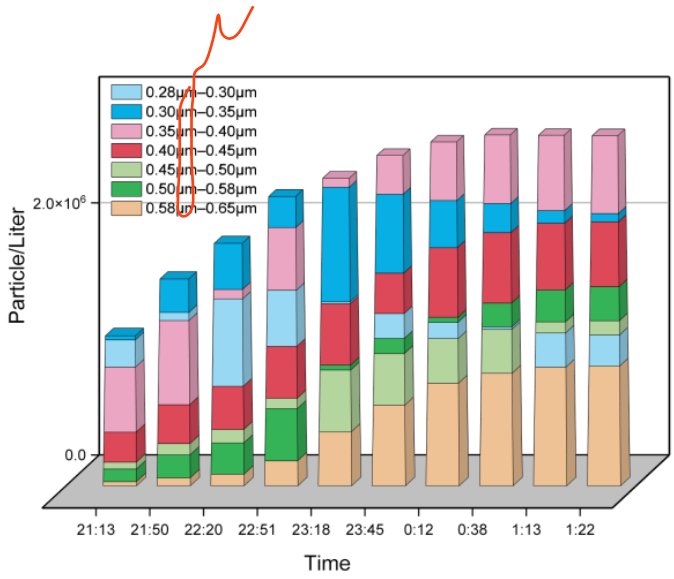
0.28μm–0.30μm
0.30μm–0.35μm
0.35μm–0.40μm
0.40μm–0.45μm
0.45μm–0.50μm
0.50μm–0.58μm
0.58μm–0.65μm
Particle/Liter
2.0×10^6
0.0
21:13
21:50
22:20
22:51
23:18
23:45
0:12
0:38
1:13
1:22
Time

(a)

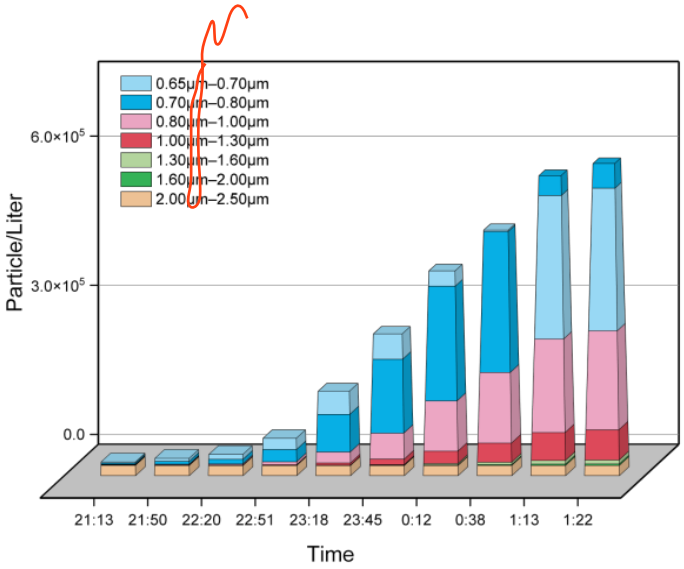
0.65μm–0.70μm
0.70μm–0.80μm
0.80μm–1.00μm
1.00μm–1.30μm
1.30μm–1.60μm
1.60μm–2.00μm
2.00μm–2.50μm
Particle/Liter
6.0×10^5
3.0×10^5
0.0
21:13
21:50
22:20
22:51
23:18
23:45
0:12
0:38
1:13
1:22
Time

(b)

Fig. 4.

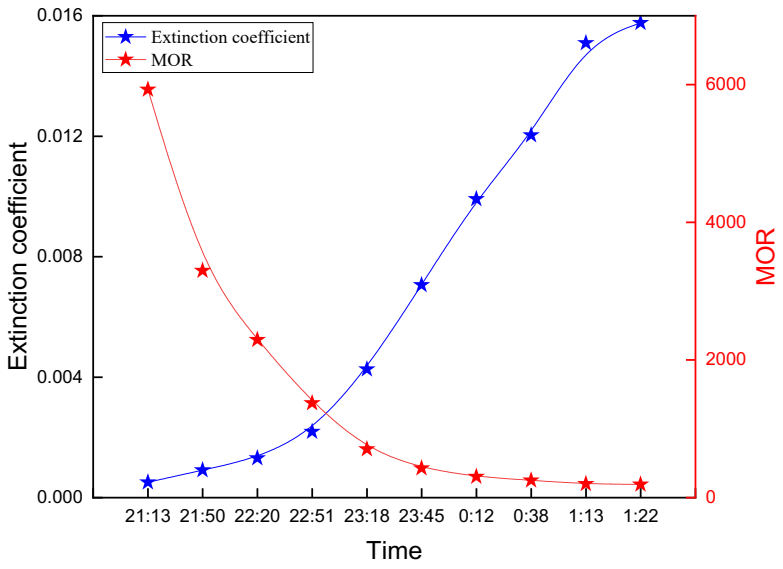
Extinction coefficient
MOR
0.016
0.012
0.008
0.004
0.000
6000
4000
2000
0
21:13
21:50
22:20
22:51
23:18
23:45
0:12
0:38
1:13
1:22
Time

Fig. 5.

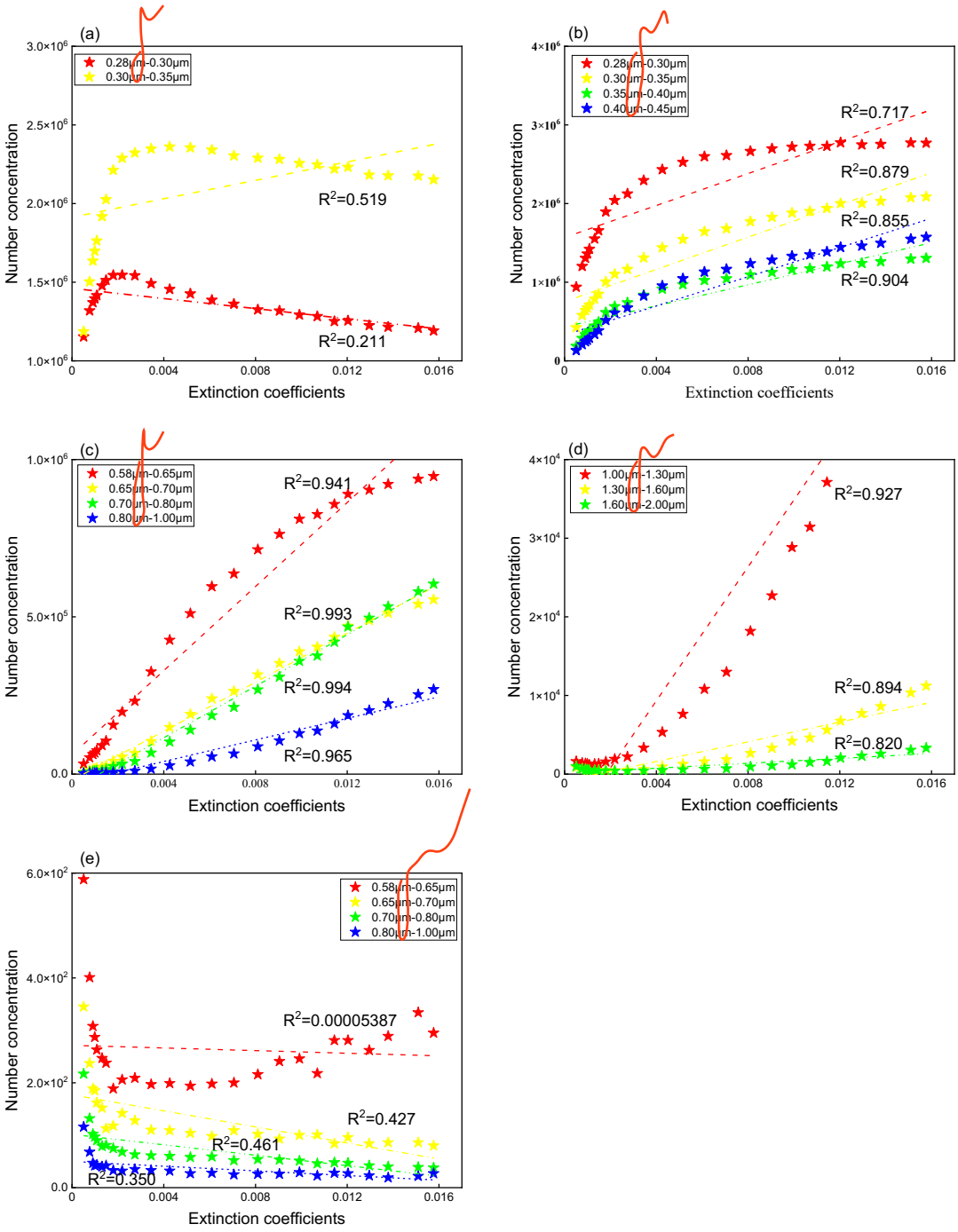
(a)
0.28μm-0.30μm
0.30μm-0.35μm
R²=0.519
R²=0.211
Number concentration
Extinction coefficients
(b)
0.28μm-0.30μm
0.30μm-0.35μm
0.35μm-0.40μm
0.40μm-0.45μm
R²=0.717
R²=0.879
R²=0.855
R²=0.904
Number concentration
Extinction coefficients
(c)
0.58μm-0.65μm
0.65μm-0.70μm
0.70μm-0.80μm
0.80μm-1.00μm
R²=0.941
R²=0.993
R²=0.994
R²=0.965
Number concentration
Extinction coefficients
(d)
1.00μm-1.30μm
1.30μm-1.60μm
1.60μm-2.00μm
R²=0.927
R²=0.894
R²=0.820
Number concentration
Extinction coefficients
(e)
0.58μm-0.65μm
0.65μm-0.70μm
0.70μm-0.80μm
0.80μm-1.00μm
R²=0.00005387
R²=0.427
R²=0.461
R²=0.350
Number concentration
Extinction coefficients

Fig. 6.

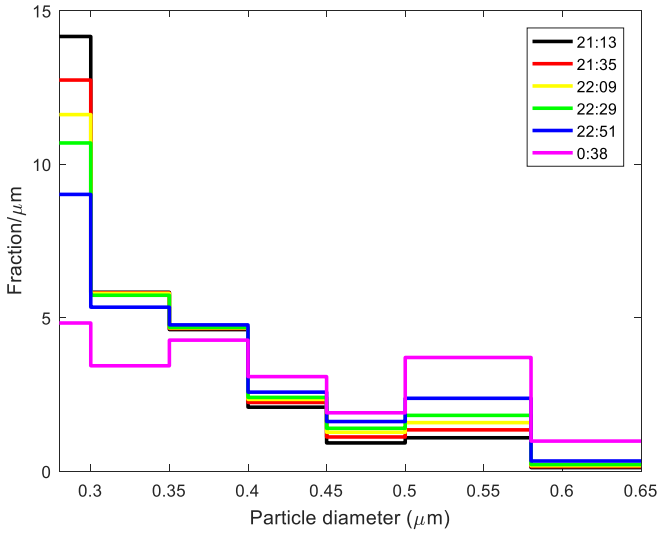
15
10
5
0
Fraction/μm
0.3
0.35
0.4
0.45
0.5
0.55
0.6
0.65
Particle diameter (μm)
21:13
21:35
22:09
22:29
22:51
0:38

(a)

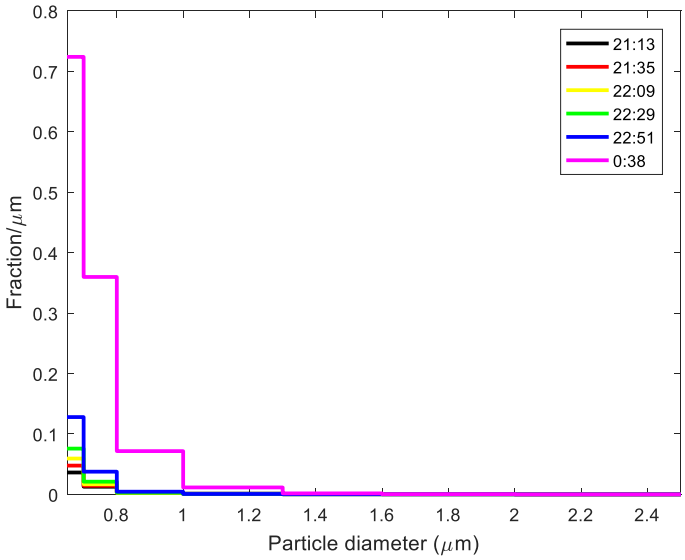
0.8
0.7
0.6
0.5
0.4
0.3
0.2
0.1
0
Fraction/μm
0.8
1
1.2
1.4
1.6
1.8
2
2.2
2.4
Particle diameter (μm)
21:13
21:35
22:09
22:29
22:51
0:38

(b)

Fig. 7.

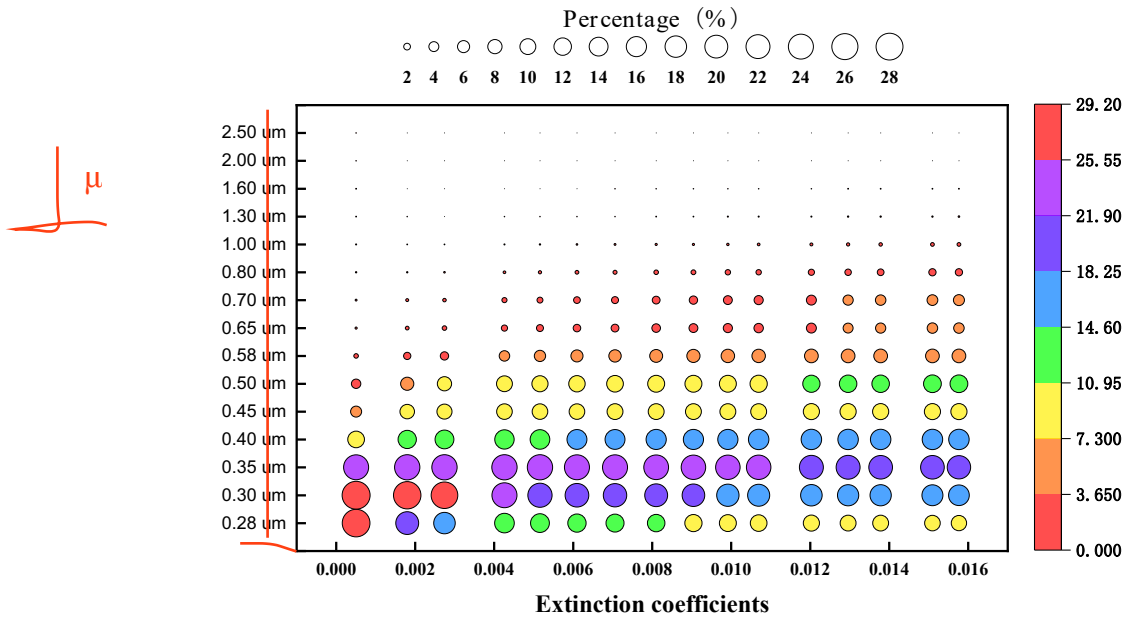
Percentage (%)
2 4 6 8 10 12 14 16 18 20 22 24 26 28
μ
2.50 um
2.00 um
1.60 um
1.30 um
1.00 um
0.80 um
0.70 um
0.65 um
0.58 um
0.50 um
0.45 um
0.40 um
0.35 um
0.30 um
0.28 um
0.000 0.002 0.004 0.006 0.008 0.010 0.012 0.014 0.016
Extinction coefficients
29.20
25.55
21.90
18.25
14.60
10.95
7.300
3.650
0.000

Fig. 8.

заменить u на μ

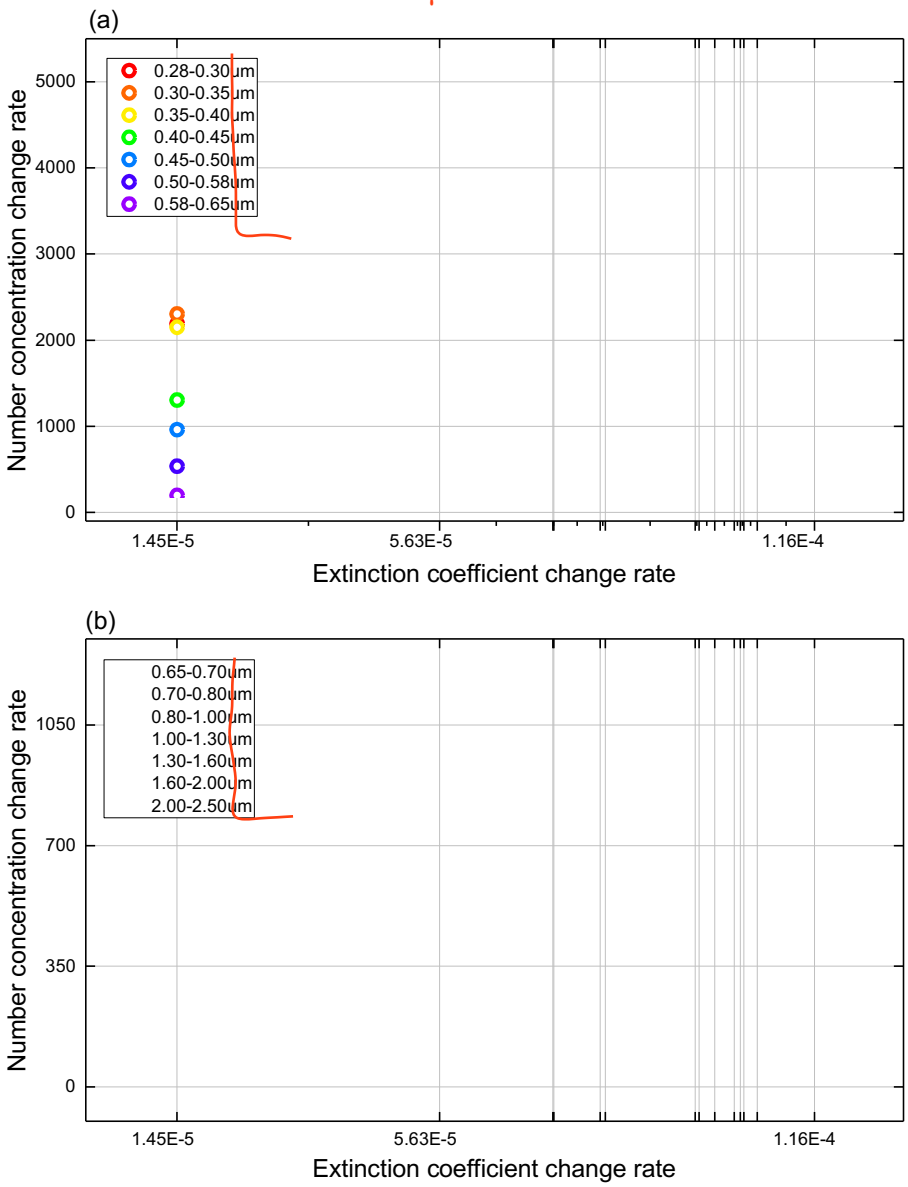

Fig. 9.

Hong-Da Tai

Email: hdtai@cauc.edu.cn

Wei Zhong

E-mail: 271955481@qq.com

Yuan Wang

E-mail: YuanWang55@outlook.com

Email: 2022031043@cauc.edu.cn

Phone: 15628975301

Yi Li

Email: 12965105@qq.com

Zi-Bo Zhuang

Email: zbzhuang@cauc.edu.cn

Pak-Wai Chan

Email: pwchan@hko.gov.hk